

Arachidonic Acid Promotes Intestinal Regeneration by Activating WNT Signaling

Qingyu Wang,¹ Yingying Lin,¹ Xiaole Sheng,³ Jiuzhi Xu,³ Xuening Hou,³ Yuan Li,¹ Hao Zhang,¹ Huiyuan Guo,¹ Zhengquan Yu,^{2,3} and Fazheng Ren^{1,2,*}

¹Key Laboratory of Functional Dairy, Beijing Laboratory of Food Quality and Safety, College of Food Science & Nutritional Engineering, China Agricultural University, Beijing, China

²Key Laboratory of Precision Nutrition and Food Quality, Department of Nutrition and Health, China Agricultural University, Beijing, China

³State Key Laboratories for Agrobiotechnology, College of Biological Sciences, China Agricultural University, Beijing, China

*Correspondence: renfazheng@cau.edu.cn

<https://doi.org/10.1016/j.stemcr.2020.06.009>

SUMMARY

Intestinal regeneration is crucial for functional restoration after injury, and nutritional molecules can play an important role in this process. Here, we found that arachidonic acid (AA) serves as a direct proliferation promoter of intestinal epithelial cells that facilitates small intestinal regeneration in both three-dimensional cultured organoids and mouse models. As shown in the study, during post-irradiation regeneration, AA positively regulates intestinal epithelial cell proliferation by upregulating the expression of *Ascl2* and activating WNT signaling, but negatively regulates intestinal epithelial cell differentiation. AA acts as a delicate regulator that efficiently facilitates epithelial tissue repair by activating radiation-resistant *Msi1*⁺ cells rather than *Lgr5*⁺ cells, which are extensively considered WNT-activated crypt base stem cells. Additionally, short-term AA treatment maintains optimal intestinal epithelial homeostasis under physiological conditions. As a result, AA treatment can be considered a potential therapy for irradiation injury repair and tissue regeneration.

INTRODUCTION

Every day, the gastrointestinal tract welcomes food nutrients into the body, and due to the continuously active state of its primary stem cells, this tract has a rapid self-renewal rate of approximately 3–5 days (Barker et al., 2007). Intestinal stem cells (ISCs) at the intestinal crypt bottom support the upward transport of their daughter cells along the villi (Crosnier et al., 2006). Moreover, this essential organ confronts continuous potential attack or injury from bacteria, toxic factors, or special conditions, such as radiation exposure and biopsy wounds. Thus, ISCs might trigger the efficient regeneration of the epithelium, which is critical for barrier maintenance and intestinal function after injury (Lindemans et al., 2015).

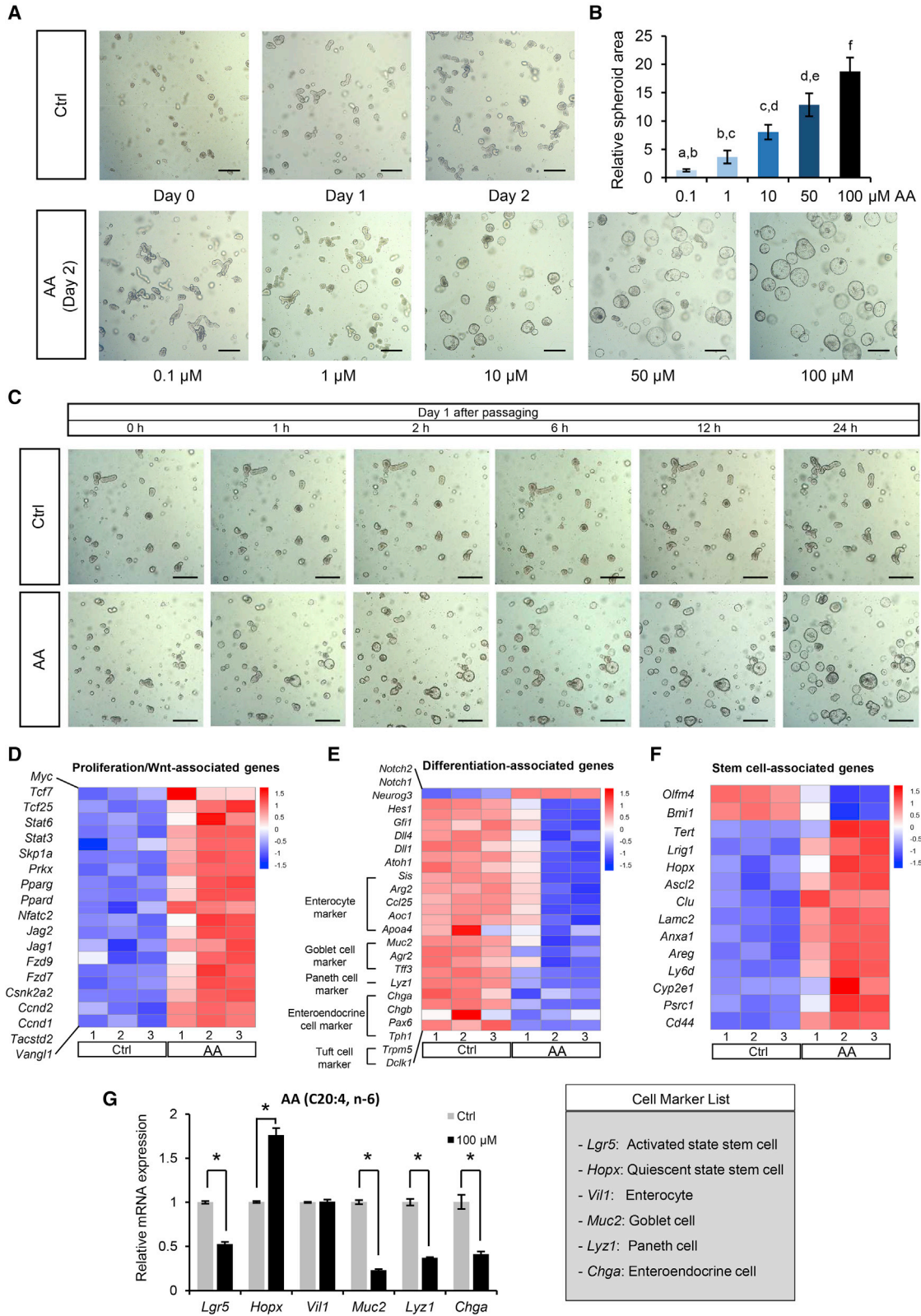
The ingested dietary molecules from the intestine might cause a physiological response that can modify the metabolism, but the mechanism through which nutritional components affect stem cell biology is not well understood. Fatty acids, which are the main component of fat, constitute an important fuel in the body that can act as a secondary messenger in physiological regulation and exerts an impact on several signaling pathways (Liscovitch and Cantley, 1994). Both clinical trials and murine models have shown that fasting can ameliorate intestinal inflammation and promote intestinal regeneration (Rangan et al., 2019); butyric acid, as one of the short-chain fatty acids, is mainly produced by intestinal microorganisms and can paradoxically sustain enterocyte growth while suppressing stem cell viability (van der Beek et al., 2017).

Additionally, the administration of mice with a high-fat diet for only 3 days will change the expression of glucose and lipid metabolism-related genes and the levels of ketogenesis-related proteins (Clara et al., 2017). An increase in dietary fat directly promotes the proliferation of ISCs and progenitor cells, which results in a higher possibility of cancer development. This result is consistent when those found for palmitic acid and stearic acid, which are the main components of high-fat diets (Beyaz et al., 2016). Because different types of fatty acids might exert multiple effects on ISC regulation, the specific functions of each type of fatty acid on ISCs would be worth studying.

In vitro cultured organoids have been widely used for studying ISC activity and tissue regeneration, as they give rise to all cell types in the intestinal epithelium and can form mini-gut-like structures (Mahe et al., 2013; Merker et al., 2016). During our preliminary screening using different types of free fatty acids (FFAs) for the treatment of organoids isolated from the murine small intestine, we found that arachidonic acid (AA) treatment induced a special spheroid phenotype rather than the budding shape observed in the control and other FFA-treated groups (Figures S1A and S1B), indicating that AA might play a role in modulating the ISC response.

As an essential fatty acid, AA is required by the majority of mammals and constitutes an important component of the outer cell membrane (Hyde and Missailidis, 2009). Along with its metabolites, AA is involved in a number of physiological functions. Previous studies have shown that AA can stimulate the proliferation of various types of stem cells,





(legend on next page)



such as hematopoietic stem cells, mesenchymal stem cells, and embryonic stem cells (Rashid et al., 2016). Additionally, an upregulated concentration of AA has been detected in colon cancer tissue, which suggests that AA might have a pro-proliferation function in the intestine (Hiraide et al., 2016). However, the available evidence regarding ISC is limited. Previous study on one of the AA metabolites has shown that the treatment of jejunum-derived budding organoids with prostaglandin E₂ (PGE₂) can induce a spheroid phenotype with a more differentiated state that is negative for 5-ethynyl-2'-deoxyuridine (Miyoshi et al., 2017).

Here, we assessed the proliferative and regenerative function of AA on the intestinal epithelium using both *in vitro* and *in vivo* models. The results showed that AA promoted the proliferation and facilitated the recovery of the small intestinal epithelium from high-dose (12 Gy) irradiation (IR) injury by elevating the *Ascl2* expression level, which synergistically triggers WNT signaling. Moreover, the regenerative effect of AA on the intestinal epithelium involved the preferential regulation of *Msi1*⁺ radiation-resistant cells, rather than *Lgr5*⁺ cells, and this finding represents a potential mechanism of intestinal regeneration.

RESULTS

AA Promotes the Proliferation of Small Intestine Epithelial Cells

To determine the function of different types of fatty acids on intestinal epithelial cells, we utilized a three-dimensional cultured intestinal organoid model that mimics the progress of regeneration. Compared with other types of fatty acids, AA treatment (50 or 100 μM, 3 days) modified the normal budding organoid into a spheroid shape (Figures S1A and S1B). The relative spheroid area of the organoids increased significantly in a dose-dependent manner, and their morphology started to change within 1 h after AA treatment (Figures 1A–1C). Given this rapid change in

morphology, we subsequently performed a transcriptome analysis of organoids treated or not treated with AA. The transcriptomes showed that AA treatment upregulated proliferation-related genes, including WNT signaling target genes (Figure 1D) (Roche et al., 2015; Beyaz et al., 2016), and downregulated differentiation-related genes, including markers of enterocytes, goblet cells, Paneth cells, enteroendocrine cells, and tuft cells (Figure 1E) (Ayyaz et al., 2019). AA treatment exerted different effects on ISC-related markers, i.e., this treatment downregulated the active-state ISC marker (*Olfm4*) and partially upregulated the reserve ISC markers (*Tert*, *Lrig1*, and *Hopx*) (Figure 1F) (Roche et al., 2015). Additionally, AA also upregulated stem cell-associated genes that have been previously found to be highly expressed 3 days after 12 Gy IR injury (*Clu*, *Lamc2*, *Anxa1*, *Areg*, and *Ly6d*) (Figure 1F) (Ayyaz et al., 2019). To validate the transcriptome data, a qRT-PCR analysis showed a mostly consistent mRNA expression pattern: AA downregulated the expression of *Lgr5*, a marker gene of active ISCs, and several genes of differentiated cells, such as *Muc2*, *Chga*, and *Lyz* (Figure 1G). Of note, *Hopx*, which is the marker gene of radiation-resistant reserve ISCs, was upregulated by AA (Figure 1G). Taken together, the transcriptome and qRT-PCR results suggest that AA might play a role in cell proliferation.

To further confirm this hypothesis, we performed immunofluorescence staining using the cell-cycling state marker KI67 (Figures 2A and 2B) and the stem/progenitor cell marker *Sox9* (Figures 2D and 2E) (Roche et al., 2015; Schell et al., 2017) and found a significantly higher percentage of KI67⁺ cells and SOX9⁺ cells after AA treatment (100 μM). This result is consistent with the qRT-PCR data, which showed that AA treatment (100 μM) significantly upregulated the mRNA expression levels of *Mki67* and *Sox9* (Figures 2C and 2F).

Consistent with the pro-proliferation function of AA, we found that the protein levels of the intestinal secretory

Figure 1. AA Induces Organoids to Form Spheroids and Alters the Transcriptome

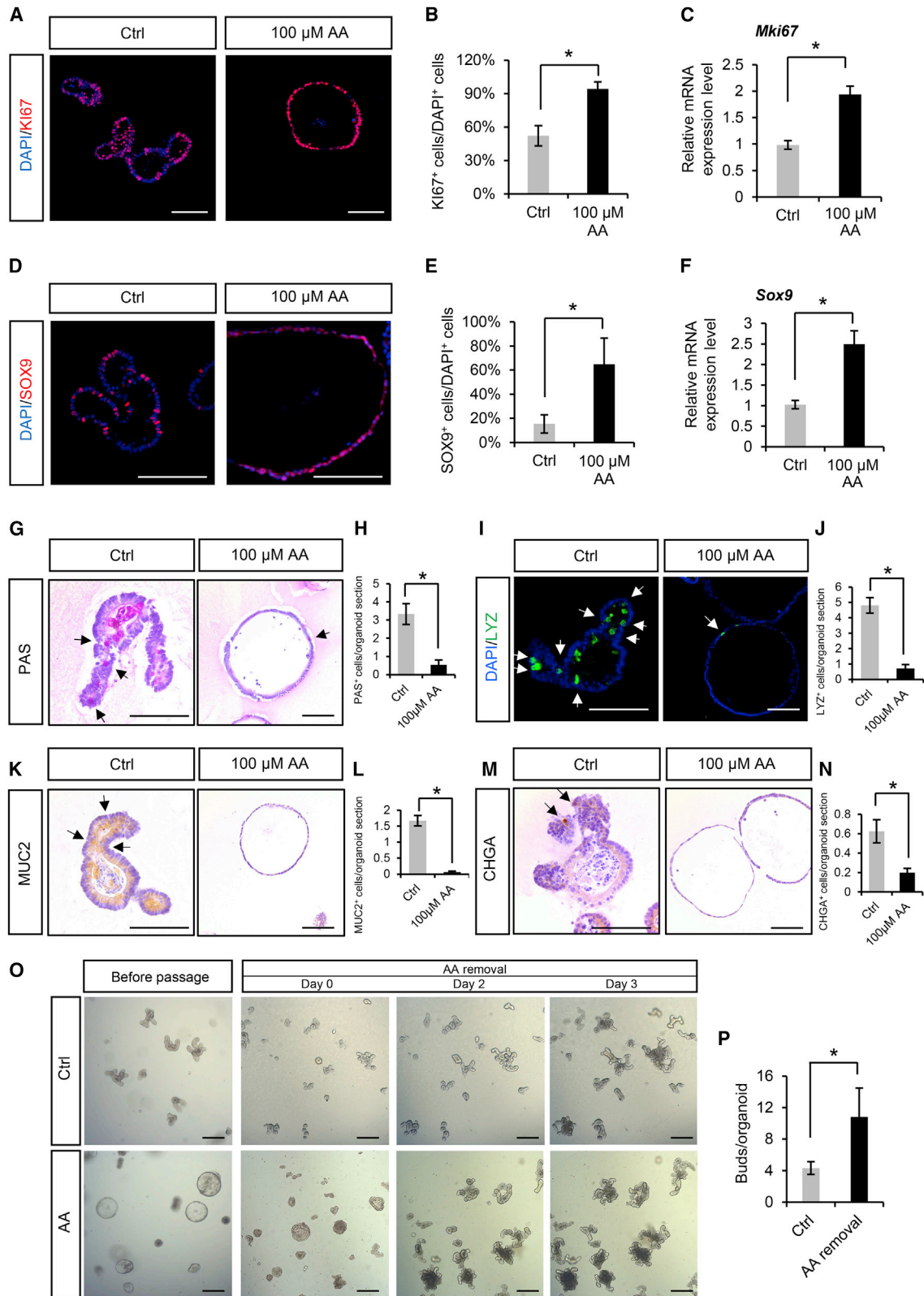
(A) Representative images of the dose effects of the AA treatments. Scale bars, 100 μm.

(B) Quantification of the average spheroid areas after treatment with different concentrations of AA.

(C) Representative images of the onset time after AA treatment (100 μM). The images at the various time points were obtained from the same well. Scale bars, 100 μm.

(D–F) Heatmaps showing the significant ($p_{\text{adj}} < 0.05$) differentially expressed genes between the control and AA treatment groups identified based on FPKM (fragments per kilobase per million mapped reads) values. Three biological replicates were included in each group, as shown in the columns. The red and blue colors indicate upregulated and downregulated genes, respectively. The scale showed the row Z score. A transcriptome analysis was performed using mRNA isolated from organoids.

(G) Relative mRNA expression levels of cell markers after AA treatment (100 μM) of organoids isolated from the murine small intestine. The control group was treated with 0.1% EtOH. Organoids derived from three animals served as independent biological replicates of each group, and more than 20 organoids were counted. Values are expressed as the mean ± SD. Statistical analysis was performed by one-way ANOVA and Tukey's post hoc test (in B; lowercase letters indicate significant differences, $p < 0.05$) and Student's t test (in G; asterisk indicates a significant difference, $*p < 0.05$). AA, arachidonic acid; Ctrl, control; CBC, crypt base columnar; EtOH, ethanol. See also Figure S1.



(legend on next page)



lineages (MUC2, LYZ, and CHGA) were downregulated after AA treatment (Figures 2G–2N). Periodic acid-Schiff (PAS) stains both goblet cells and Paneth cells, which is a validation of the combined immunostaining results of MUC2 and LYZ. These results were consistent with the mRNA expression levels obtained from both the transcriptome analysis and the qRT-PCR validation (Figures 1E and 1G). Additionally, to examine whether the spheroid phenotype would persist after the removal of AA, we subsequently withdrew AA from the culture system after the spheroids had formed. The spheroids returned to a robust budding phenotype within 48 h, which suggested that AA is rapidly metabolized and the pro-proliferation effect is reversible (Figure 2O). Moreover, the return of the spheroids to normal growth media resulted in a significantly higher crypt number than that obtained with normal budding organoids, which suggested that AA treatment induced a more proliferated cell state within spheroids (Figure 2P).

AA Induces Small Intestine Epithelium Regeneration after IR Injury

After identifying the growth-promoting effect of AA in the organoid culture system, we used an IR injury model to further confirm the function of AA *in vivo*. IR injury is the gold-standard model for investigating the regenerative response of ISCs by depleting rapidly cycling ISCs (Richmond et al., 2016). After optimizing the AA concentration in both serum and the fecal content, we intragastrically treated mice with 10 mg/mouse AA per day (Figures S2A and S2B). After 12 Gy IR, the body weight and food intake of the mice were significantly decreased (Figures S2C and S2D), and significant intestinal shortening was observed compared with the control group (Figure S2E). According to the H&E staining results, the structure of the duodenum

was markedly destroyed after 12 Gy treatment, whereas no significant differences were found between the normal AA feeding group and the control group, as shown by the quantification of the villi heights (Figures S3A and S3B). Following 12 Gy IR, the AA treatment group had a significantly higher crypt depth than the 12 Gy-injured control group, which suggested that the AA-treated group exhibited a stronger recovery capacity (Figure S3C). KI67 is expressed by cells in an activated state of proliferation and is used to identify regenerative crypts (Otsuka and Suzuki, 2016). We found that regenerative crypts started to appear on day 3 (Figure S3E). To identify whether AA exerts a protective effect against IR injury, we stained cleaved CASPASE-3, which is a marker of the activation of the apoptosis cascade (Roche et al., 2015), and found that the apoptotic extent of the control and AA-treated groups was the same (Figures S3F–S3H). On day 4 after 12 Gy IR, significantly more regenerative crypts were found in the AA treatment group (Figure 3B). This increase in KI67⁺ regenerative crypts was observed throughout the length of the small intestine and was most robust in the duodenum (Figure 3C), indicating that the duodenum is the most sensitive area to AA-induced crypt regeneration. Moreover, the KI67⁺ cell-distribution pattern revealed a significantly higher number of crypts with more KI67⁺ cells in the duodenum, which indicated that the duodenum is more sensitive to the AA-induced regenerative effect (Figure 3D).

With respect to the differentiation state, the PAS and immunostaining results indicated that the position of the differentiated cells in the regenerative crypts after AA treatment was mostly equal to that of the cells in the control group (Figures 3E, 3G, 3I, and 3K). Additionally, the AA treatment group contained slightly more PAS⁺ cells per crypt and the same numbers of MUC2⁺ and LYZ⁺ cells (Figures 3F, 3H,

Figure 2. AA Promotes Proliferation while Inducing a Low Level of Differentiation of Small Intestinal Organoids

- (A) Representative images of KI67 staining of organoids treated with 100 μ M AA. KI67⁺ cells represent proliferative cells.
(B) Quantification of the distribution of KI67⁺ cells in AA-treated organoids.
(C) Relative mRNA expression level of *Mki67* after treatment with different concentrations of AA.
(D) Representative images of SOX9 staining of organoids treated with 100 μ M AA. SOX9⁺ cells represent stem/progenitor cells.
(E) Quantification of the distribution of SOX9⁺ cells in AA-treated organoids.
(F) Relative mRNA expression level of *Sox9* after treatment with different concentrations of AA.
(G, I, K, and M) Representative images of differentiated lineage staining of organoids treated with 100 μ M AA. Representative positive cells are marked by black or white arrows.
(H, J, L, and N) Quantification results of the differentiated lineage staining of organoids treated with 100 μ M AA. The y axes represent the positive cells per section of organoids.
(O) Representative images of the AA withdrawal assay. After 3 days of AA treatment (100 μ M), the organoids were integrally transferred to AA-free Matrigel and chased for 3 days.
(P) Quantification of the crypt number per organoid obtained from 3 days after the removal of AA.
The control group was treated with 0.1% EtOH. Organoids derived from three animals served as independent biological replicates of each group, and more than 20 organoids were counted. Values are expressed as the mean \pm SD. Data were statistically analyzed using Student's t test (significant difference, * p < 0.05). AA, arachidonic acid; Ctrl, control; EtOH, ethanol. Scale bars, 100 μ m.

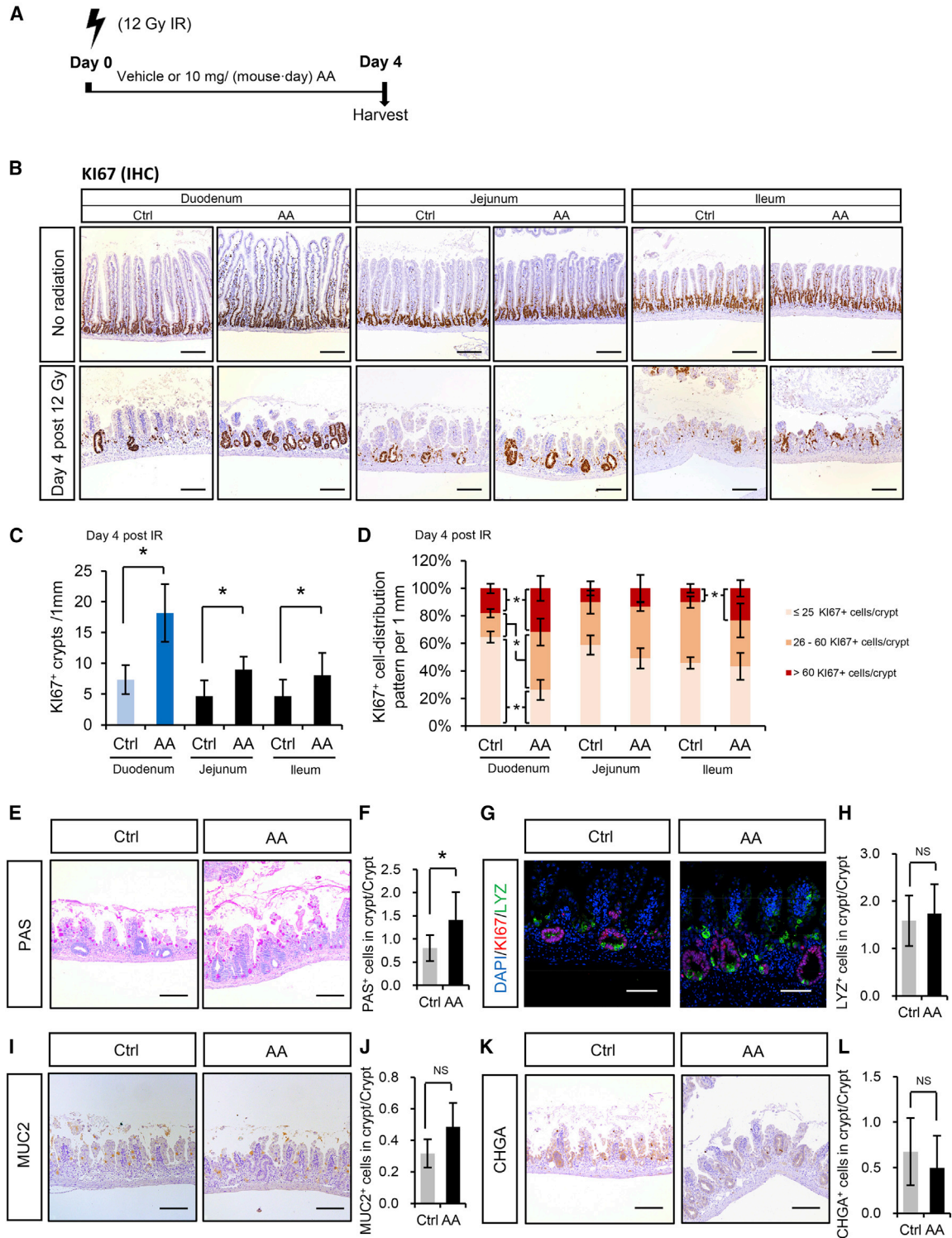


Figure 3. AA Promotes Small Intestine Epithelium Regeneration after 12 Gy IR Injury

(A) Schematic of the IR injury model.

(B) Representative images of IHC staining of KI67 in different parts of the small intestine on 4 days after 12 Gy IR and AA treatment (10 mg/mouse per day). Scale bars, 200 μ m.

(C) Quantification of KI67⁺ crypts per 1-mm tissue section from different parts of the small intestine (n = 3 biological replicates).

(legend continued on next page)



3J, and 3L), which suggested that AA promotes the formation of functional regenerative crypts rather than inducing the tissue into an abnormal tumorigenic state. Taken together, the results suggest that AA aids tissue regeneration and promotes small intestine recovery following IR injury.

AA Aids Maintenance of Small Intestine Function

After demonstrating that AA plays a potent role in IR injury recovery, we focused on whether AA exerts a growth-promoting effect on the regular renewal of small intestine tissue. AA treatment was administered for 1 week through continuous gavage once per day (10 mg/mouse). AA treatment did not change the morphology and distribution of differentiation lineages along the crypt-villus axes compared with the control treatment (Figures S4B–S4I). No additional apoptosis was found, as demonstrated by cleaved CASPASE-3 staining (Figures S4J and S4K). Moreover, AA treatment exerted no significant effect on WNT signaling activation under normal conditions (Figure S4L). To assess the migration speed of the cells (Nalapareddy et al., 2017), we performed a one-pulse bromodeoxyuridine (BrdU) assay. The data revealed that the average travel time of BrdU-positive cells from the crypt base to the top of villi was 3 days post BrdU administration, and this finding was obtained from both the control and experimental groups, which suggested that short-term continuous AA feeding under physiological conditions did not significantly change the proliferation state of stem/progenitor cells (Figure S4M). Therefore, the results obtained under physiological conditions suggest that short-term AA treatment maintains the homeostasis of the small intestine.

AA Promotes Proliferation by Activating WNT Signaling

The analysis of the mRNA transcriptome showed that several WNT signaling-related transcription factors were upregulated in AA-treated organoids (Figure 1D), which suggested that AA might function by activating WNT signaling. To evaluate this hypothesis, we used the rat small intestinal epithelial cell line 6 (IEC-6), which shares good characteristics with small intestine transit-amplifying (TA) cells (Quaroni et al., 1979). A cell counting kit-8 (CCK-8) assay showed that AA gradually increased the viability of the cells in a dose-dependent manner (Figure 4A) without inducing cell apoptosis (Figures S5A and S5B). AA upregulated WNT-

related proteins (CYCLIN D1 and β -CATENIN), downregulated the phosphorylated form of GSK3 β (p-GSK3 β), which is a WNT antagonist, and also downregulated the phosphorylated form of β -CATENIN (p- β -CATENIN) (Figure 4B). The lesser degradation of cytoplasmic β -CATENIN leads to nuclear β -CATENIN accumulation and consequently activates WNT signaling (Castellone et al., 2005). To further confirm this observation, we performed a TOPFlash/FOPFlash assay, whose results showed that AA treatment stimulated the expression of a β -CATENIN/TCF/LEF-dependent reporter gene system (Figure 4C).

We subsequently used *Axin2*-LacZ transgenic mice, which contain a WNT signaling reporter, to verify the results *in vivo* with an IR injury model. After 12 Gy IR injury and intragastric injection of AA for 3 days, the AA treatment group tended to produce higher numbers of LacZ⁺ cells and LacZ⁺ crypts than the non-treated group, which demonstrated that AA can activate WNT signaling within the regenerative crypts (Figures 4D–4F).

Ascl2 Is Involved in AA-Induced WNT Activation

Because the qRT-PCR validation results revealed that *Ascl2* exhibited the most sensitive response among all WNT signaling-related genes (Figure 5A), we further explored its role in the WNT signaling pathway after AA treatment. Among three pairs of small interfering RNAs (siRNAs) targeting *Ascl2*, si-*Ascl2*-2 exhibited the highest knockdown efficiency at the mRNA expression level (Figure S5F). We then used si-*Ascl2*-2 to downregulate *Ascl2* expression in the IEC-6 cell line at both the transcriptional and translational levels (Figures 5B and 5C). In addition to *Ascl2* itself, the expression levels of WNT target genes (*Axin2* and *Ccnd1* mRNA, and AXIN2 and CYCLIN D1 protein) were significantly decreased by si-*Ascl2*-2 interference, which indicated that *Ascl2* might participate in the regulation of WNT signaling (Figures 5B, 5D, and 5E). Moreover, AA treatment significantly rescued the interference of *Ascl2* and the mRNA expression of WNT target genes (*Axin2* and *Ccnd1*) in a dose-dependent manner (Figures 5C–5E). The altered protein levels of WNT-related genes were all rescued after AA treatment, regardless of the dose (Figure 5B). Collectively, the results showed that AA treatment rescued the deficiency in WNT signaling following *Ascl2* depletion, which indicated that *Ascl2* is highly correlated with AA-induced WNT signaling activation.

(D) Quantification of KI67⁺ cell-distribution pattern in different parts of the small intestine (n = 3 biological replicates).

(E, G, I, and K) Representative images of differentiated lineages and KI67⁺ regenerative crypts in the duodenum 3 days post 12 Gy IR injury and AA treatment (10 mg/mouse per day). The scale bars for PAS, MUC2, and CHGA represent 200 μ m. The scale bars for LYZ represent 100 μ m.

(F, H, J, and L) Quantification of differentiated lineage staining (n = 3 biological replicates).

Values are expressed as the mean \pm SD. Data were statistically analyzed using Student's t test (significant difference, *p < 0.05). AA, arachidonic acid; Ctrl, control; IHC, immunohistochemistry; IR, irradiation. See also Figures S2 and S3.

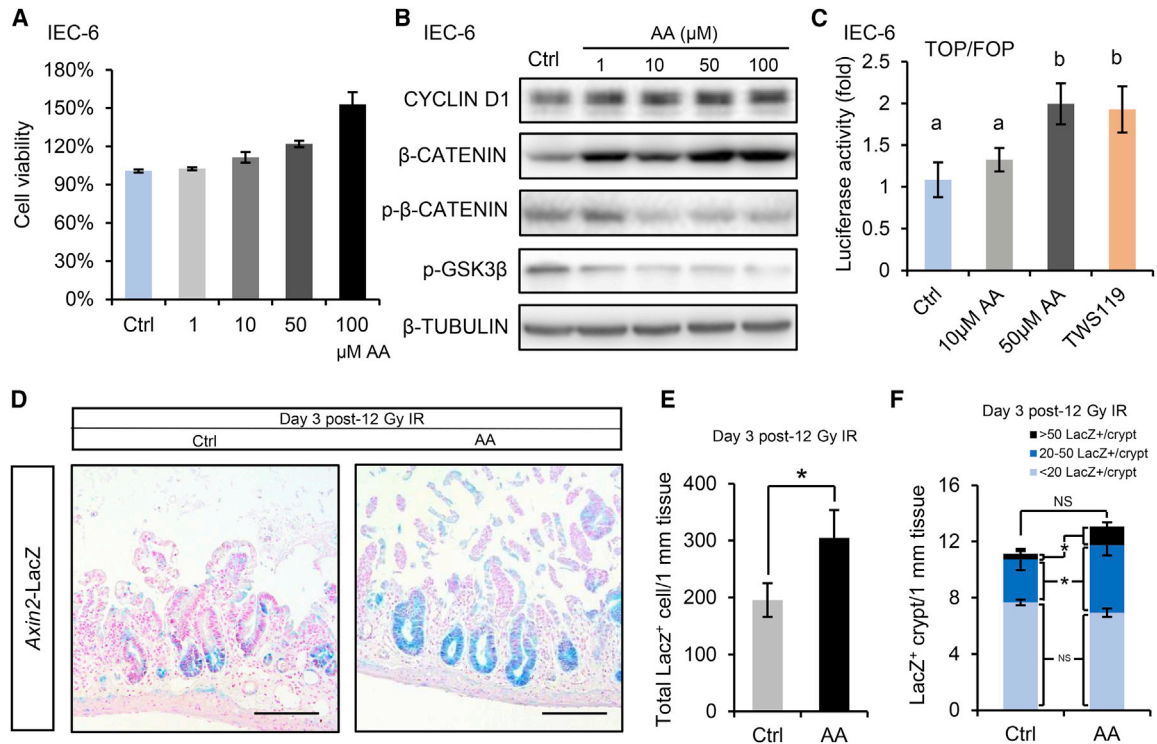


Figure 4. AA Promotes the Regeneration of Small Intestine Epithelial Cells by Activating the WNT Signaling Pathway

(A) Cell viability of IEC-6 cells after treatments with different AA concentrations. The viability of the control group (0.1% EtOH) was considered to be 100% (n = 5 individual wells).

(B) Representative western blot images of the IEC-6 cells after 24 h of AA treatment (n = 3 individual experiments).

(C) TOPFlash/FOPFlash reporter assay. TWS119 is a WNT signaling activator that served as the positive control (n = 3 individual experiments).

(D) Representative images of duodenal parts from *Axin2*-LacZ transgenic mice 3 days after 12 Gy IR injury and 10 mg AA/(mouse · day) AA treatment. Scale bars, 200 μm.

(E and F) Quantification of LacZ staining 3 days after 12 Gy IR (n = 3 biological replicates and littermates).

Values are expressed as the mean ± SD. Data were statistically analyzed using Student's t test (E and F; the asterisk indicates a significant difference, *p < 0.05) and one-way ANOVA with Tukey's post hoc test (C; lowercase letters indicate significant differences, p < 0.05). AA, arachidonic acid; IEC-6, rat small intestinal epithelial crypt cell; EtOH, ethanol; IR, irradiation; NS, not significant.

AA Promotes Intestinal Regeneration by Activating *Msi1*⁺ Cells

Because a previous study has shown that *Lgr5*⁺ ISCs are indispensable for IR-induced intestinal regeneration (Metcalfe et al., 2014), and *Lgr5* itself is not only a WNT target gene but also constitutes a component of the WNT receptor (De Lau et al., 2011), we hypothesized that AA acts to rebuild the structure of the small intestine after IR injury by activating *Lgr5*⁺ cells. To investigate this hypothesis, we treated *Lgr5*-EGFP transgenic mice with AA and analyzed the changes in their *Lgr5*⁺ populations by flow cytometry. AA treatment led to a significant decrease in the number of *Lgr5*⁺ cells both under physiological conditions and after high-dose IR (Figures 6A–6D), which is consistent with the mRNA expression results obtained with the organoid model (Figure 1G). Additionally, an *in vitro* time

course assay showed that the *Lgr5* mRNA expression level was markedly decreased after 6 h of AA treatment (p < 0.05) and then remained at a stable low level at later time points, which suggested that the organoids undergo constant rapid proliferation of TA cells after 6 h of incubation with AA (Figure S1C). We then performed Cre-mediated genetic tracing of *Msi1*-CreERT;R26LacZ transgenic mice, in which *Msi1*⁺ cells have been preliminarily proven to be radiation-resistant crypt cells (Yousefi et al., 2016). Under normal conditions, 3 days of AA treatment activated the *Msi1*⁺ cells to produce significantly more immediate daughters than those observed in the control group (Figures 6G and 6H). Moreover, after 12 Gy IR, the AA treatment group exhibited a significantly higher number of LacZ⁺ crypts, which indicated that AA promotes intestinal regeneration by activating *Msi1*⁺ cells (Figures 6E and 6F).

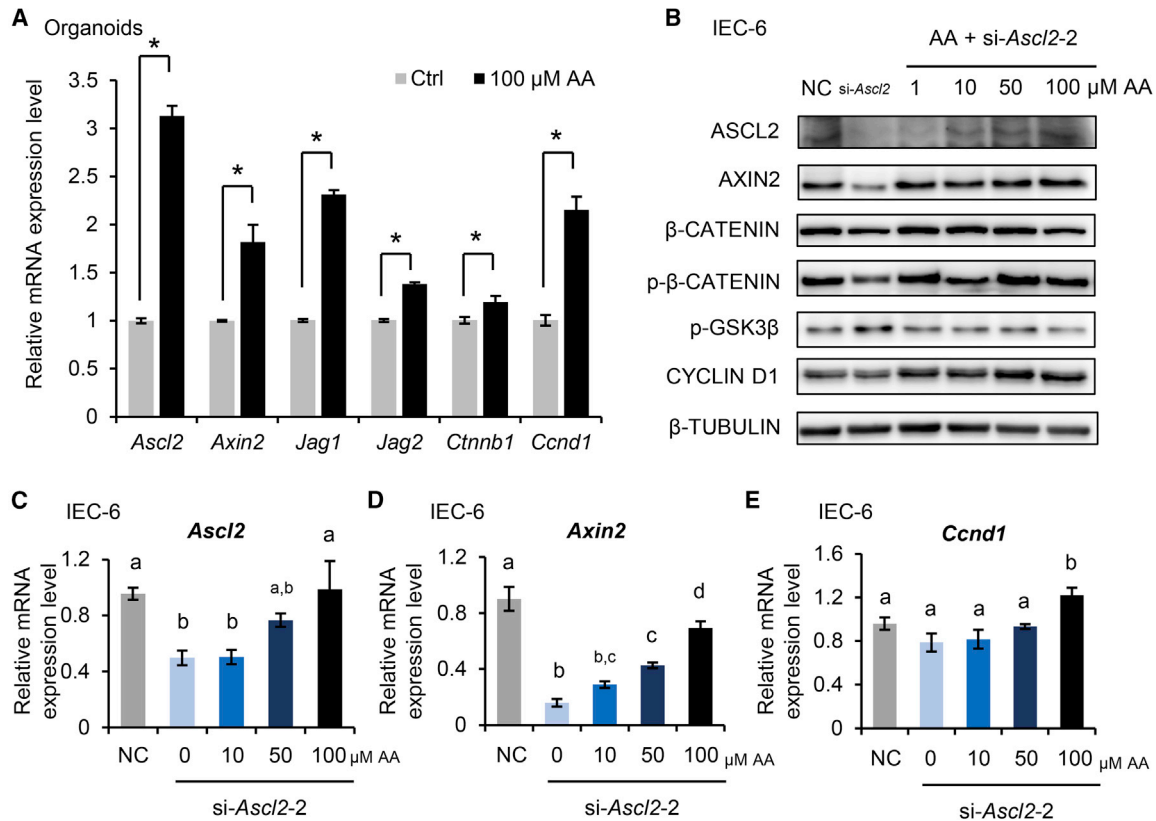


Figure 5. AA Triggers the Expression of *Ascl2* and Activates the WNT Signaling Pathway

(A) Relative mRNA expression level of WNT signaling-related genes in 100 μM AA-treated organoids isolated from the small intestine (n = 3 biological replicates).

(B) Representative western blot results of IEC-6 cells treated with si-*Ascl2*-2 and different doses of AA (n = 3 individual experiments).

(C–E) qRT-PCR results of *Ascl2* and WNT target genes in the IEC-6 cells after si-*Ascl2*-2 interference and treatment with different doses of AA (n = 3 individual experiments).

Values are expressed as the mean ± SD. Data were statistically analyzed using Student's t test (A; the asterisk indicates a significant difference, *p < 0.05) and one-way ANOVA with Tukey's post hoc test (C, D, and E; lowercase letters indicate significant differences, p < 0.05). AA, arachidonic acid; IEC-6, rat small intestinal epithelial crypt cell; NC, non-specific control. See also Figure S5.

DISCUSSION

In the present study, AA induced a marked spheroid phenotype characterized by a more active cell-cycling status, a higher proportion of stem/progenitor cells, and fewer differentiated lineages. These findings appear to be the opposite from those obtained in a previous study, which showed that one of the metabolites of AA, PGE₂, induces the differentiation of organoids toward the same spheroid phenotype (Miyoshi et al., 2017). The difference might be because PGE₂ is formed via the cyclooxygenase pathway, whereas the lipoxygenase pathway was also shown to be involved in AA metabolism and could contribute to cell proliferation (Figures S6A and S6B) (Hyde and Missailidis, 2009). However, the exact mechanism underlying AA metabolites participating in AA-induced intestinal epithelial

proliferation needs further determination. In addition, the morphology change might be explained by AA- or PGE₂-mediated activation of ion channels (Tallima and El Ridi, 2018).

Under IR injury and normal physiological conditions, the number of *Lgr5*⁺ crypt base columnar (CBC) cells was significantly reduced in response to AA treatment. Likewise, the expression level of *Lgr5* was reduced in the organoid model upon AA treatment. Our findings showed that AA promotes cell proliferation during intestinal regeneration and concomitantly reduces *Lgr5*⁺ stem cells. In support of this notion, a recently published study has indicated that the loss of *Lgr5* expression correlates with fast proliferation in organoids (Serra et al., 2019). It is also consistent with prior single-cell transcriptome data showing that organoids in a more proliferative state have

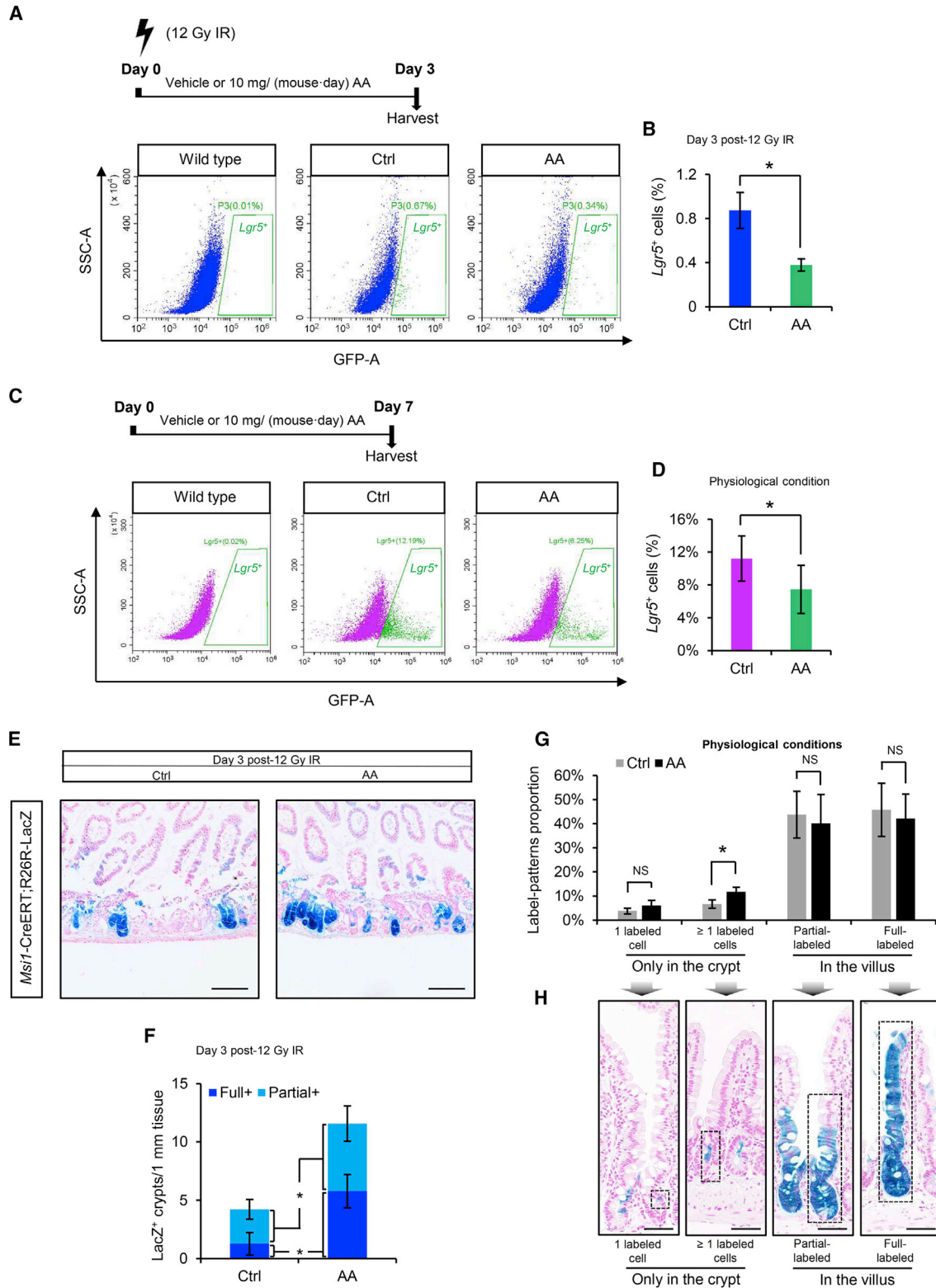


Figure 6. AA Activates WNT Signaling Independent of *Lgr5*⁺ Cells but Might Act through *Msi1*⁺ Cells

(A) Representative images of flow cytometry. Three days of 10 mg/(mouse·day) AA treatment after 12 Gy IR injury.

(B) Quantification of flow cytometry in the radiation-induced injury experiment (n = 6 biological replicates).

(legend continued on next page)



fewer *Lgr5*⁺ cells but more TA compartments when compared with organoids grown in differentiation-promoting culture medium (Fujii et al., 2018). AA might promote intestinal regeneration by enhancing the proliferation of *Lgr5*⁻ intestinal stem/progenitor cells. Indeed, cellular plasticity has been proved in several lineages residing above the crypt base and contributes to intestinal regeneration. *Dll1*⁺ or *Atoh1*⁺ secretory progenitors and *Alpi*⁺ enterocyte progenitors have been shown to possess renewal capacity and were able to compensate for the complete ablation of *Lgr5*⁺ cells under physiological or regenerative conditions (Castillo-Azofeifa et al., 2019; Tetteh et al., 2016; van Es et al., 2012). Another recent study showed that the post-IR regeneration of intestinal epithelium preferentially went through the activation of crypt *Clu*⁺ cells rather than the recruitment of depleted *Lgr5*⁺ cells (Ayyaz et al., 2019). In addition, our findings suggested that radiation-resistant *Msi1*⁺ crypt cells also contribute to intestinal regeneration and that this process is reinforced by AA treatment. Of note, we are not ruling out the importance of *Lgr5*⁺ stem cells in contributing to intestinal regeneration (Metcalf et al., 2014) because *Lgr5*⁺ cells remain at an extremely low but existent level after AA treatment. Taken together, AA promotes intestinal regeneration by favorably activating *Msi1*⁺ cells rather than *Lgr5*⁺ ISCs, and the cellular mechanism needs further investigation.

Canonical WNT pathway activity is a major driving force for regeneration after injury (Clevers et al., 2014). Here, we demonstrated that AA promotes intestinal regeneration by activating the WNT signaling pathway. However, we also noticed that the expression level of *Lgr5*, a WNT target gene, and *Lgr5*⁺ cells decreased in response to AA treatment. In agreement with our findings, it has been implicated that *Lgr5* expression is not strictly controlled by WNT pathway activity in the intestinal crypt (Li et al., 2016). An unknown inhibitory mechanism might exist to suppress *Lgr5* expression under WNT activation conditions. For example, bone morphogenetic protein restricts

the *Lgr5*⁺ population independent of WNT signaling, indicating a regulation bypass between *Lgr5* and WNT signaling (Qi et al., 2017). In contrast to *Lgr5*, another WNT target gene, *Ascl2* (van der Flier et al., 2009), was up-regulated by AA treatment. Indeed, a recent study indicated that *Ascl2*-dependent dedifferentiation of crypt progenitors occurs in almost all regeneration after ISC injury, and emerging cells express *Ascl2* but not *Lgr5* at the beginning of the regenerative process (Murata et al., 2020), although *Ascl2* and *Lgr5* have been reported to be highly coexpressed in normal physiology (Roche et al., 2015). It appears that AA promotes intestinal regeneration via *Ascl2* activation, rather than *Lgr5*.

In summary, our findings reveal a conclusion regarding the mechanism through which one type of FFA, AA, promotes intestinal regeneration following injury and maintains a good homeostatic function of the small intestine epithelium under physiological conditions. The results demonstrate that AA can trigger the expression of *Ascl2* and activate WNT signaling. In addition, AA promotes intestinal regeneration through a group of radiation-resistant *Msi1*⁺ cells rather than *Lgr5*⁺ ISCs, which provides the potential regenerative mechanisms in the intestine. Elucidating the role of AA in regulating intestinal epithelial cells would not only improve our understanding of tissue homeostasis but also yield promising therapeutic strategies for injury repair.

EXPERIMENTAL PROCEDURES

Crypt Isolation

Small intestine crypts were isolated according to previous methods (Beyaz et al., 2016). In brief, the mouse proximal small intestines were flushed with ice-cold Dulbecco's PBS (DPBS). The villi were removed by scraping with a coverslip and leaving the crypts attached. The intestine was then cut into pieces with a length of approximately 1–2 mm and incubated in Gentle cell dissociation reagent (STEMCELL Technologies, #07174) for 15 min at room temperature. After the

(C) Representative images of flow cytometry. Normal physiological conditions were administered with 7 days of 10 mg/(mouse·day) AA treatment.

(D) Quantification of flow-cytometry results after AA treatment under normal physiological conditions (n = 6 biological replicates).

(E) Representative images of LacZ staining of the duodenum of the *Msi1*-CreERT;R26RLacZ transgenic mouse model. Scale bars, 200 μm.

(F) Quantification of the LacZ⁺ fully labeled crypts (Full⁺) and LacZ⁺ partially labeled crypts (Partial⁺) per 1-mm tissue section (n = 3 biological replicates; littermates).

(G) Quantification of the short-term lineage-tracing labeling pattern in the duodenum. *Msi1*-CreERT;R26RLacZ transgenic mice were induced with tamoxifen for 15 h following 10 mg/(mouse·day) AA treatment for 3 days under physiological conditions. The right sides of the fully cut crypt-villus axes were counted.

(H) Representative images of the labeling pattern in the short-term lineage-tracing experiments. The standard counting pattern for each type is shown in the dashed box. Scale bars, 50 μm.

Values are expressed as the mean ± SD. Data were statistically analyzed using Student's t test (significant difference, *p < 0.05). AA, arachidonic acid; Ctrl, control; IR, irradiation; NS, not significant.



fractions settled the supernatant was removed, and 10 mL of DPBS with 10% fetal bovine serum (FBS) was added and pipetted up and down with a 10-mL serological pipette. The supernatant was passed through a 70- μ m strainer, and the crypt fraction was collected. The crypt purity was evaluated under a microscope.

Organoid and Cell Culture

After isolation from the mouse proximal small intestine, the crypts were resuspended in a mixture of Matrigel (Corning, #356237). The basic culture medium was growth medium (STEMCELL, #06005) with penicillin/streptomycin/gentamicin (Solarbio Life Science, #P1410). The IEC-6 cell line was purchased from American Type Culture Collection, and the cells were maintained in Dulbecco's modified Eagle's medium (DMEM) with 5% FBS, 0.1 units/mL insulin, and 100 units/mL penicillin-streptomycin. Similar densities of spheroids or cells were seeded for all the experiments. AA (Sigma, #A3611) was dissolved in cold 0.1% EtOH, and 0.1% EtOH was used as a control.

Cell Viability Assay

Cell viability was measured using an enhanced CCK-8 (Beyotime Biotechnology, #C0042). IEC-6 cells were seeded in a 96-well plate at a density of 5×10^3 cells/well, and 24 h after plating, AA was added to the medium; 0.1% ethanol was used as a control. After another 24 h of incubation, 10 μ L of CCK-8 reagent was added to each well. The optical density at 450 nm was read using a microplate reader (Tecan, Austria). The cell proliferation rate of the control group was defined as 100%.

RNA Extraction, RT-PCR, RNA-Seq, and Transcriptome Analysis

Total extracted RNA from the treated small intestinal epithelial organoids was collected 3 days after passaging using an RNAPrep pure Micro Kit (Tiangen Biotech [Beijing], #DP420). RNA samples from the IEC-6 cell line after 24 h of treatment were prepared using TRIzol reagent (Invitrogen, #15596-026). The RNA quantity was assessed using a NanoDrop spectrophotometer (Tecan). Reverse transcription was performed using 1 μ g of total RNA with All-In-One RT MasterMix (Applied Biological Materials, #G486), and qRT-PCR was then performed using SYBR Premix Ex Taq (Takara, #RR420A). The primer sequences are listed in Table S1. The relative expression levels were normalized to those of *Gapdh*. The RNA-sequencing (RNA-seq) experiments of the organoids were performed by Novogene (Beijing, China). Sequencing libraries were generated using the NEBNext Ultra RNA Library Prep Kit for Illumina (NEB, USA), and index codes were added to attribute sequences to each sample. After the index-coded samples were clustered on a cBot Cluster Generation System using TruSeq PE Cluster Kit v3-cBot-HS (Illumina), the libraries were prepared using an Illumina NovaSeq 6000 platform. The sequencing depth was 6 GB per sample, and Fa (ftp://ftp.ensembl.org/pub/release-91/fasta/mus_musculus/dna/) and Gtf (ftp://ftp.ensembl.org/pub/release-91/gtf/mus_musculus/) were used as the reference genomes. The p values were adjusted using the Benjamini-Hochberg method.

siRNA Transfection

The siRNAs targeting *Ascl2* and non-specific control were transfected into IEC-6 cells cultured in 24-well plates using Lipofectamine 2000 transfection reagent (Invitrogen, #11668030) according to the manufacturer's directions. One day after the cells were plated, AA was added to the culture medium and the cells were treated for 24 h. Cell lysates were generated using TRIzol reagent (Invitrogen, #15596-026) and then subjected to total RNA extraction using the aforementioned protocol. The transfection efficiency was measured by flow cytometry and microscopy. The siRNA sequences are listed in Table S2.

TOPFlash Reporter Assay

IEC-6 cells were suspended in serum/antibiotic-free DMEM at a concentration of 1.25×10^7 cells/mL. The plasmids were transfected by electroporation using a Nucleofector 2b device (Lonza, AAB-1001) with the D-032 program. Two micrograms of TOPFlash or FOPFlash plasmid and 1 μ g of TK were added to the transfection system. The transfected cells were plated in 24-well plates for 8 h, and the medium was changed to DMEM supplemented with 10% FBS and the different AA treatments. After 24 h of incubation the cells were harvested, and their luciferase activity was assayed using the Dual Luciferase Reporter Assay System (Promega, #E2920) in accordance with the manufacturer's recommended protocol (Ouko et al., 2004). The TOPFlash/FOPFlash ratios were measured to estimate the activation of WNT signaling. TWS119, which can activate WNT signaling, served as the positive control (Chen et al., 2009); the stock solution consisted of 10 mg/mL TWS119 in DMSO and was used at 1:10,000 dilution.

Histology, Immunofluorescence, and Immunohistochemistry

The organoids and intestinal tissues were fixed with 4% paraformaldehyde (PFA) in PBS overnight at 4°C, embedded in paraffin, and sectioned into 8- μ m and 5- μ m sections, respectively. After deparaffination and rehydration, the slides were stained with H&E for morphological observations. For immunofluorescence staining, the dehydrated paraffin sections were microwaved, pretreated in 0.01 M citrate buffer (pH 6.0), and incubated in blocking buffer containing 10% normal goat serum in Tris-buffered saline with Tween 20 (Cell Signaling Technology, #5425) and then with the diluted primary antibodies in blocking buffer. The sections were subsequently incubated with secondary antibodies conjugated to Alexa Fluor 488 or 594 fluorophores (Invitrogen) and counterstained with DAPI (Sigma, #D9542), and coverslips were mounted with ProLong gold antifade mountant (Thermo Fisher Scientific, #P10144). For immunohistochemistry, after incubation with the primary antibody, the sections were incubated with biotin-conjugated secondary antibodies (Vector Laboratories), and coverslips were mounted with neutral balsam (Solarbio Life Science, #G8590). The following primary antibodies were used: mouse anti-KI67 (NeoMarkers, #RM-9106-S1), rabbit anti-CASPASE-3 (Cell Signaling Technology, #9664s), rabbit anti-SOX9 (Abcam, #ab185230), mouse anti-MUC2 (Santa Cruz Biotechnology, #sc-59859), rabbit anti-CHGA (Abcam, #ab15160), and goat anti-LYZ (Santa Cruz, #sc-27958).



Periodic Acid-Schiff Staining

PAS staining was performed using a PAS stain kit (Leagene, #DG0005) according to the manufacturer's guidelines. In brief, the slides were subjected to the same hydration steps as those used in the immunostaining analysis until placement into distilled water, and the paraffin slides were then immersed in periodic acid solution for 8 min and subjected to one 3-min rinse in tap water and two 3-min rinses in distilled water. The slides were subsequently immersed in Schiff's solution for 10 min and then rinsed for 10 min with tap water. Hematoxylin staining was then performed for 30 s to stain the nucleus. After another 10-min rinse in tap water, the slides were subjected to the same steps as those used in the immunohistochemistry staining until placement in xylene and then mounted with neutral balsam.

Western Blotting

The proteins from treated cells were extracted using standard procedures. After incubation in lysis buffer (Beyotime Biotechnology, #P0013B) supplemented with protease inhibitor mixture (Solarbio Life Sciences, #P6730) and protein phosphatase inhibitor (Solarbio Life Sciences, #P1260), the protein samples were centrifuged at $14,000 \times g$ for 20 min. The protein lysates were quantified using a BCA protein assay kit (Thermo Fisher, #23225). Equivalent protein concentrations were resolved by SDS-PAGE, and the proteins were transferred to polyvinylidene difluoride (PVDF) membranes (Millipore, #IPVH00010). The PVDF membranes were blocked with 5% non-fat dry milk for 1 h at room temperature. The following antibodies were applied: rabbit anti- β -CATENIN (Abcam, #ab32572), rabbit anti-p- β -CATENIN (CST, #9561s), rabbit anti- β -TUBULIN (Cell Signaling, #2146), rabbit anti-CYCLIN D1 (Abcam, #ab134175), mouse anti-ASCL2 (Merck, #MAB4417), rabbit anti-GSK3 β (Abcam, #ab75745), and rabbit anti-AXIN2 (Abcam, #ab109307).

Animal Experiments

Male C57BL/6N mice aged 8–10 weeks were purchased from Beijing Vital River Laboratory Animal Technology and maintained in a specific pathogen-free barrier facility with a strict 12-h light cycle. *Lgr5-eGFP-CreERT2*, *Axin2-LacZ*, and *Msi1-CreERT2*; R26RLacZ transgenic mice were obtained from Zhengquan Yu's laboratory (China Agricultural University, College of Biological Sciences) as gifts. All the transgenic mice used in the experiments were littermates. For the activation of CreERT2, the mice were intraperitoneally injected with tamoxifen (4 mg/25 g body weight) 15 h prior to IR (γ -ray radiation from a ^{60}Co source, Peking University) and AA (Sigma, #A3611) treatment. AA was suspended in 1% bile salts (Sigma, #48305) using a 1-mL disposable syringe, and 1% bile salts were used as a control. All mouse experimental procedures and protocols were evaluated and authorized by the Regulations of Beijing Laboratory Animal Management and strictly followed the guidelines of the Institutional Animal Care and Use Committee of China Agricultural University.

Localization of β -Galactosidase Activity

LacZ expression was characterized by 5-bromo-4-chloro-3-indolyl- β -D-galactoside (X-Gal) staining as described previously, with slight modifications (Barker et al., 2009). The duodenal part of

the small intestine was isolated and flushed immediately with ice-cold fix solution (0.2% glutaraldehyde, 5 mM EGTA, and 2 mM MgCl_2). After incubation on ice for 2.5 h, the fixative was removed and the intestines were washed three times in wash buffer (0.02% NP40, 0.01% Na-deoxycholate, and 2 mM MgCl_2) for 30 min at room temperature. The β -galactosidase substrate (5 mM $\text{K}_3\text{Fe}(\text{CN})_6$, 5 mM $\text{K}_4\text{Fe}(\text{CN})_6 \cdot 3\text{H}_2\text{O}$, 2 mM MgCl_2 , 0.02% NP40, 0.1% Na-deoxycholate, and 1 mg/mL X-Gal) was then added, and the tissues were incubated overnight at room temperature in the dark. The substrate was removed and the tissues washed three times with PBS for 10 min at room temperature. The tissues were then fixed overnight using 4% PFA in PBS at 4°C in the dark. The PFA was removed, and the tissues were then washed three times with PBS for 20 min at room temperature. The stained tissues were then transferred and embedded in paraffin blocks. The tissue blocks for LacZ scoring were sectioned into 5- μm sections, which were then subjected to the same preparation steps until the hydration step and subsequently counterstained with neutral red.

Flow Cytometry

The dissected intestine was incubated with 5 mM EDTA and 1.5 mM dithiothreitol in Hanks balanced salt solution for 30 min on ice. To harvest the intestine under physiological conditions, we removed the villi part by scraping with coverslips. A single-cell suspension was produced following dispase (STEMCELL, #7913) treatment, and the cells were passed through a 40- μm cell strainer. The flow-cytometry analysis was performed using a CytoFLEX Flow Cytometer (Beckman Coulter). The single and propidium iodide-negative cells were selected. The fluorescein isothiocyanate-positive (FITC $^+$) cells were isolated and quantified as *Lgr5* $^+$ cells. Cell cytometry was also used to measure the efficiency of the transfection of the siRNAs into the IEC-6 cell line. The gate settings were similar to those described above. Cells that were successfully transfected were isolated and quantified as FITC $^+$ cells.

Statistical Analysis

Microsoft Excel (version 2016) and SPSS (version 13.0) were used to perform all the statistical analyses, and $p < 0.05$ was considered to indicate significance. All the samples represent biological replicates. Two-tailed Student's *t* tests were used to determine the differences in the means between two groups. Multiple comparisons among more than two groups were analyzed by one-way ANOVA. The data are presented as the mean \pm standard deviation (SD).

Data and Code Availability

RNA-seq data that support the findings of this study have been deposited in the NCBI/GEO database (<https://www.ncbi.nlm.nih.gov/geo/>) under accession number GEO: GSE146871.

SUPPLEMENTAL INFORMATION

Supplemental Information can be found online at <https://doi.org/10.1016/j.stemcr.2020.06.009>.



AUTHOR CONTRIBUTIONS

Conception and design, Q.W., Z.Y., and F.R.; Investigation and data acquisition, Q.W., Y. Lin, H.Z., H.G., and Z.Y.; Data analysis and interpretation, Q.W., Y. Lin, X.S., J.X., and X.H.; Technical and material support, Y. Li, H.Z., H.G., Z.Y., and F.R.; Writing and revision of the manuscript, Q.W., Z.Y., and F.R.; Study supervision, Z.Y. and F.R.

ACKNOWLEDGMENTS

We would like to thank the members from the laboratory animal center in China Agricultural University for their assistance with animal care. We thank Camilla Richmond for the careful review of the manuscript and invaluable suggestions. This study was supported by the No.111 project from the Ministry of Education of the People's Republic of China (No. B18053).

Received: October 26, 2019

Revised: June 9, 2020

Accepted: June 9, 2020

Published: July 9, 2020

REFERENCES

- Ayyaz, A., Kumar, S., Sangiorgi, B., Ghoshal, B., Gosio, J., Ouladan, S., Fink, M., Barutcu, S., Trcka, D., and Shen, J. (2019). Single-cell transcriptomes of the regenerating intestine reveal a revival stem cell. *Nature* 569, 121.
- Barker, N., Ridgway, R.A., van Es, J.H., van de Wetering, M., Begthel, H., van den Born, M., Danenberg, E., Clarke, A.R., Sansom, O.J., and Clevers, H. (2009). Crypt stem cells as the cells-of-origin of intestinal cancer. *Nature* 457, 608.
- Barker, N., Van Es, J.H., Kuipers, J., Kujala, P., Van Den Born, M., Cozijnsen, M., Haegebarth, A., Korving, J., Begthel, H., and Peters, P.J. (2007). Identification of stem cells in small intestine and colon by marker gene *Lgr5*. *Nature* 449, 1003.
- Beyaz, S., Mana, M.D., Roper, J., Kedrin, D., Saadatpour, A., Hong, S.-J., Bauer-Rowe, K.E., Xifaras, M.E., Akkad, A., and Arias, E. (2016). High-fat diet enhances stemness and tumorigenicity of intestinal progenitors. *Nature* 531, 53.
- Castellone, M.D., Teramoto, H., Williams, B.O., Druet, K.M., and Gutkind, J.S. (2005). Prostaglandin E2 promotes colon cancer cell growth through a Gs-axin- β -catenin signaling axis. *Science* 310, 1504–1510.
- Castillo-Azofeifa, D., Fazio, E.N., Nattiv, R., Good, H.J., Wald, T., Pest, M.A., de Sauvage, F.J., and Klein, O.D. (2019). *Atoh1*⁺ secretory progenitors possess renewal capacity independent of *Lgr5*⁺ cells during colonic regeneration. *EMBO J.* 38, e99984.
- Chen, M., Philipp, M., Wang, J., Premont, R.T., Garrison, T.R., Caron, M.G., Lefkowitz, R.J., and Chen, W. (2009). G Protein-coupled receptor kinases phosphorylate LRP6 in the Wnt pathway. *J. Biol. Chem.* 284, 35040–35048.
- Clara, R., Schumacher, M., Ramachandran, D., Fedele, S., Krieger, J.P., Langhans, W., and Mansouri, A. (2017). Metabolic adaptation of the small intestine to short-and medium-term high-fat diet exposure. *J. Cell. Physiol.* 232, 167–175.
- Clevers, H., Loh, K.M., and Nusse, R. (2014). An integral program for tissue renewal and regeneration: Wnt signaling and stem cell control. *Science* 346, 1248012.
- Crosnier, C., Stamatakis, D., and Lewis, J. (2006). Organizing cell renewal in the intestine: stem cells, signals and combinatorial control. *Nat. Rev. Genet.* 7, 349.
- De Lau, W., Barker, N., Low, T.Y., Koo, B.-K., Li, V.S., Teunissen, H., Kujala, P., Haegebarth, A., Peters, P.J., and Van De Wetering, M. (2011). *Lgr5* homologues associate with Wnt receptors and mediate R-spondin signalling. *Nature* 476, 293.
- Fujii, M., Matano, M., Toshimitsu, K., Takano, A., Mikami, Y., Nishikori, S., Sugimoto, S., and Sato, T. (2018). Human intestinal organoids maintain self-renewal capacity and cellular diversity in niche-inspired culture condition. *Cell Stem Cell* 23, 787–793.e6.
- Hiraide, T., Ikegami, K., Sakaguchi, T., Morita, Y., Hayasaka, T., Masaki, N., Waki, M., Sugiyama, E., Shinriki, S., and Takeda, M. (2016). Accumulation of arachidonic acid-containing phosphatidylinositol at the outer edge of colorectal cancer. *Sci. Rep.* 6, 29935.
- Hyde, C., and Missailidis, S. (2009). Inhibition of arachidonic acid metabolism and its implication on cell proliferation and tumour-angiogenesis. *Int. Immunopharmacol.* 9, 701–715.
- Li, N., Yousefi, M., Nakauka-Ddamba, A., Tobias, J.W., Jensen, S.T., Morrissey, E.E., and Lengner, C.J. (2016). Heterogeneity in readouts of canonical wnt pathway activity within intestinal crypts. *Dev. Dyn.* 245, 822–833.
- Lindemans, C.A., Calafiore, M., Mertelsmann, A.M., O'connor, M.H., Dudakov, J.A., Jenq, R.R., Velardi, E., Young, L.F., Smith, O.M., and Lawrence, G. (2015). Interleukin-22 promotes intestinal-stem-cell-mediated epithelial regeneration. *Nature* 528, 560.
- Liscovitch, M., and Cantley, L.C. (1994). Lipid second messengers. *Cell* 77, 329–334.
- Mahe, M.M., Aihara, E., Schumacher, M.A., Zavros, Y., Montrose, M.H., Helmuth, M.A., Sato, T., and Shroyer, N.F. (2013). Establishment of gastrointestinal epithelial organoids. *Curr. Protoc. Mouse Biol.* 3, 217–240.
- Merker, S.R., Weitz, J., and Stange, D.E. (2016). Gastrointestinal organoids: how they gut it out. *Dev. Biol.* 420, 239–250.
- Metcalf, C., Kljavin, N.M., Ybarra, R., de Sauvage, and Frederic, J. (2014). *Lgr5*⁺ stem cells are indispensable for radiation-induced intestinal regeneration. *Cell Stem Cell* 14, 149–159.
- Miyoshi, H., VanDussen, K.L., Malvin, N.P., Ryu, S.H., Wang, Y., Sonnek, N.M., Lai, C.W., and Stappenbeck, T.S. (2017). Prostaglandin E2 promotes intestinal repair through an adaptive cellular response of the epithelium. *EMBO J.* 36, 5–24.
- Murata, K., Jadhav, U., Madha, S., van Es, J., Dean, J., Cavazza, A., Wucherpfennig, K., Michor, F., Clevers, H., and Shivdasani, R.A. (2020). *Ascl2*-dependent cell dedifferentiation drives regeneration of ablated intestinal stem cells. *Cell Stem Cell* 26, 377–390.e6.
- Nalapareddy, K., Nattamai, K.J., Kumar, R.S., Karns, R., Wikenheiser-Brokamp, K.A., Sampson, L.L., Mahe, M.M., Sundaram, N., Yacyshyn, M.-B., and Yacyshyn, B. (2017). Canonical Wnt signaling ameliorates aging of intestinal stem cells. *Cell Rep.* 18, 2608–2621.
- Otsuka, K., and Suzuki, K. (2016). Differences in radiation dose response between small and large intestinal crypts. *Radiat. Res.* 186, 302–314.



- Ouko, L., Ziegler, T.R., Gu, L.H., Eisenberg, L.M., and Yang, V.W. (2004). Wnt11 signaling promotes proliferation, transformation, and migration of IEC6 intestinal epithelial cells. *J. Biol. Chem.* *279*, 26707–26715.
- Qi, Z., Li, Y., Zhao, B., Xu, C., Liu, Y., Li, H., Zhang, B., Wang, X., Yang, X., Xie, W., et al. (2017). BMP restricts stemness of intestinal Lgr5⁺ stem cells by directly suppressing their signature genes. *Nat. Commun.* *8*, 13824.
- Quaroni, A., Wands, J., Trelstad, R.L., and Isselbacher, K.J. (1979). Epithelioid cell cultures from rat small intestine. Characterization by morphologic and immunologic criteria. *J. Cell Biol.* *80*, 248–265.
- Rangan, P., Choi, I., Wei, M., Navarrete, G., Guen, E., Brandhorst, S., Enyati, N., Pasia, G., Maesincee, D., and Ocon, V. (2019). Fasting-mimicking diet modulates microbiota and promotes intestinal regeneration to reduce inflammatory bowel disease pathology. *Cell Rep.* *26*, 2704–2719. e6.
- Rashid, M.A., Haque, M., and Akbar, M. (2016). In *The Benefits of Natural Products for Neurodegenerative Diseases*, M.M. Essa, M. Akbar, and G. Guillemin, eds. (Springer), pp. 367–380.
- Richmond, C.A., Shah, M.S., Carlone, D.L., and Breault, D.T. (2016). An enduring role for quiescent stem cells. *Dev. Dyn.* *245*, 718–726.
- Roche, K.C., Gracz, A.D., Liu, X.F., Newton, V., Akiyama, H., and Magness, S.T. (2015). SOX9 maintains reserve stem cells and preserves radioresistance in mouse small intestine. *Gastroenterology* *149*, 1553–1563.e10.
- Schell, J.C., Wisidagama, D.R., Bensard, C., Zhao, H., Wei, P., Tanner, J., Flores, A., Mohlman, J., Sorensen, L.K., and Earl, C.S. (2017). Control of intestinal stem cell function and proliferation by mitochondrial pyruvate metabolism. *Nat. Cell Biol.* *19*, 1027.
- Serra, D., Mayr, U., Boni, A., Lukonin, I., Rempfler, M., Challet Meylan, L., Stadler, M.B., Strnad, P., Papasaikas, P., Vischi, D., et al. (2019). Self-organization and symmetry breaking in intestinal organoid development. *Nature* *569*, 66–72.
- Tallima, H., and El Ridi, R. (2018). Arachidonic acid: physiological roles and potential health benefits—a review. *J. Adv. Res.* *11*, 33–41.
- Tetteh, P.W., Basak, O., Farin, H.F., Wiebrands, K., Kretschmar, K., Begthel, H., van den Born, M., Korving, J., de Sauvage, F., van Es, J.H., et al. (2016). Replacement of lost Lgr5-positive stem cells through plasticity of their enterocyte-lineage daughters. *Cell Stem Cell* *18*, 203–213.
- van der Beek, C.M., Dejong, C.H., Troost, F.J., Masclee, A.A., and Lenaerts, K. (2017). Role of short-chain fatty acids in colonic inflammation, carcinogenesis, and mucosal protection and healing. *Nutr. Rev.* *75*, 286–305.
- van der Flier, L.G., van Gijn, M.E., Hatzis, P., Kujala, P., Haegerbarth, A., Stange, D.E., Begthel, H., van den Born, M., Guryev, V., and Oving, I. (2009). Transcription factor achaete scute-like 2 controls intestinal stem cell fate. *Cell* *136*, 903–912.
- van Es, J.H., Sato, T., van de Wetering, M., Lyubimova, A., Yee Nee, A.N., Gregorieff, A., Sasaki, N., Zeinstra, L., van den Born, M., Korving, J., et al. (2012). Dll1⁺ secretory progenitor cells revert to stem cells upon crypt damage. *Nat. Cell Biol.* *14*, 1099–1104.
- Yousefi, M., Li, N., Nakauka-Ddamba, A., Wang, S., Davidow, K., Schoenberger, J., Yu, Z., Jensen, S.T., Kharas, M.G., and Lengner, C.J. (2016). Msi RNA-binding proteins control reserve intestinal stem cell quiescence. *J. Cell Biol.* *215*, 401–413.